

PCCP

Accepted Manuscript



This is an *Accepted Manuscript*, which has been through the Royal Society of Chemistry peer review process and has been accepted for publication.

Accepted Manuscripts are published online shortly after acceptance, before technical editing, formatting and proof reading. Using this free service, authors can make their results available to the community, in citable form, before we publish the edited article. We will replace this *Accepted Manuscript* with the edited and formatted *Advance Article* as soon as it is available.

You can find more information about *Accepted Manuscripts* in the [Information for Authors](#).

Please note that technical editing may introduce minor changes to the text and/or graphics, which may alter content. The journal's standard [Terms & Conditions](#) and the [Ethical guidelines](#) still apply. In no event shall the Royal Society of Chemistry be held responsible for any errors or omissions in this *Accepted Manuscript* or any consequences arising from the use of any information it contains.



PCCP

ARTICLE

Predictive Morphology, Stoichiometry and Structure of Surface Species in Supported Ru Nanoparticles under H₂ and CO atmospheres from Combined Experimental and DFT Studies

Received 18th August 2015,
Accepted 00th January 20xx

DOI: 10.1039/x0xx00000x

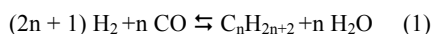
www.rsc.org/

Alex Comas-Vives,^{a*} Karol Furman^a, David Gajan^b, M. Cem Akatay,^c Anne Lesage^b, Fabio H. Ribeiro,^c Christophe Copéret^{a*}

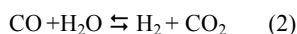
Further understanding of the chemisorption properties towards CO and H₂ on silica-supported Ru nanoparticles is crucial in order to rationalize their high activity towards methanation, Fischer Tropsch and Water Gas Shift reactions. Ru nanoparticles having the same chemisorption properties towards CO and H₂ were synthesized on different silica-based supports in order to combine various analytical techniques and obtain complimentary detailed information on their structure; while silica spheres were used in order to obtain High-Resolution TEM images of the Ru nanoparticles, high surface area silica-based material (SBA) allowed CO chemisorption to be monitored by ¹³C NMR spectroscopy. In addition, a model of the hcp-based Ru nanoparticles observed by HR-TEM was used to predict by *ab initio* calculations the CO and H₂ coverages on the Ru nanoparticle under different conditions of interest in catalysis. For both adsorbates we show and quantify how the adsorption properties of the nanoparticle differ from the commonly used slab models. For the case of CO we show how the top, bridge and hollow sites can be present on the Ru nanoparticle, providing a description at atomistic level in good agreement with the IR spectroscopy measurements.

Introduction

Supported metal nanoparticles (NPs) are one of the largest classes of heterogeneous catalysts being used both in the petrochemical and the fine chemical industries.^{1,2} They are particularly important in the field of energy and selective hydrogenation. For instance, they play an essential role in the production of hydrogen and methanol or in the Gas-to-Liquid process,^{3,4} in which hydrogen and carbon monoxide are converted into long alkane or alkene chains via the Fischer-Tropsch (FT) reaction (1) with a particular case called methanation producing methane and water (*n* = 1).⁵



Another important example is the Water Gas Shift (WGS) reaction (2),⁶ which allows producing H₂ from the reaction of H₂O and CO or modulating the H₂/CO ratio.



^a ETH Zürich, Department of Chemistry and Applied Biosciences, Vladimir-Prelog-Weg 1-5, CH-8093 Zürich, Switzerland.

^b Centre de RMN à Très Hauts Champs Institut des Sciences Analytiques Université de Lyon (CNRS/ENS Lyon/UCB Lyon 1) 5, rue de la Doua, 69100 Villeurbanne, France

^c Purdue University, School of Chemical Engineering, Forney Hall of Chemical Engineering, 480 Stadium Mall Drive, West Lafayette, IN 47907-2100, USA.

Electronic Supplementary Information (ESI) available: See DOI: 10.1039/x0xx00000x

Of the many metals, Ru exhibits high activity and selectivity towards long chain hydrocarbons in FT.^{7,8} In these systems, there are numerous parameters influencing the catalyst performances, such as the size and the distribution of the metallic nanoparticles, but also their interaction with the support.^{9,10}

One of the main methods to characterize and understand the chemistry of supported nanoparticles is the use of H₂ and CO chemisorption.¹¹⁻¹³ As for other metals the chemisorption stoichiometry of supported Ru nanoparticles towards small molecules like H₂ and CO highly depend on the support.^{14,15,16,17} In addition even for SiO₂, for which no strong-metal-support-interaction and spillover¹⁸ is expected, a variety of H₂ adsorption stoichiometry has been reported. We have previously demonstrated that fully characterized (EXAFS, TEM, XPS) 2–nm silica-supported Ru nanoparticles adsorb ca. 2H per surface Ru atoms,¹⁹ a value much larger than what is expected from hydrogen adsorption stoichiometry on flat surfaces.^{20, 21} Obvious questions related to such systems are: i) what are the natural adsorption state(s) – structures – and stoichiometries of hydrogen and CO on (supported) metal particles such as Ru nanoparticles, and ii) how/why their adsorption differ from simple slab models.¹⁹ With the development of more powerful tools and the continuous increase in computational power, DFT calculations are more and more used to provide a deeper understanding of metallic surfaces and nanoparticles in order to understand their chemisorption properties and their reactivity in catalytic transformations.²²⁻²⁵ Original studies on the adsorption properties of metal nanoparticles focused on

ideal surfaces, but the significant difference observed between flat ideal surfaces and nanoparticles is striking.²⁶⁻²⁹ For instance, *ab initio* calculations have shown that the adsorption energies of a CO molecules on Ru nanoparticles can be stronger than on the Ru001 by ca. 11 kcal.mol⁻¹.²⁷ In addition, *fcc*-based Ru nanoparticles were found to adsorb higher CO per Ru surface atom than the ideal *hcp*-Ru001 surface: 1.5 ML vs ca. 0.8 ML, respectively.²⁶ Besides the role of the steps in the CO activation,³⁰⁻³² and the role of water in FT,³³ the CO coverage on the nanoparticle and the assistance by H₂ in the CO cleavage has been suggested to play a key role in the Fischer-Tropsch reaction,²⁶ and hence a more profound understanding of the chemisorption not only of CO but also of H₂ is needed.

In order to address these questions, here we have prepared narrowly dispersed 1.6 nm Ru nanoparticles on three types of silica supports (SiO₂, SBA-15 and SiO₂-spheres), which have been characterized by combining Transmission Electron Microscopy (TEM) with chemisorption studies, IR and NMR spectroscopies. We have previously shown that these silica-supported Ru nanoparticles of 1-2 nm particle size are active towards the methanation reaction, a particular case of the FT reaction with $n=1$.¹⁰ While the Ru nanoparticles on the three different supports present similar CO and H₂ stoichiometry per surface metallic Ru atom, as evidenced from chemisorption experiments and IR spectroscopy, the different morphology of the support allows one to get access to complementary detailed structural information. Thus, the particle shape is obtained from HR-TEM of Ru NPs supported on silica-spheres, while the high surface area support – SBA-15 – allows monitoring CO chemisorption by ¹³C NMR. Finally, we carefully investigated the CO and H₂ chemisorption on model nanoparticles by DFT calculations. After determining the preferred particle shape, the energetics of CO and H₂ coverages on the nanoparticles for a wide range of temperatures and pressures was obtained by DFT calculations and compared with experiment. The synergy between different complementary experimental and computational techniques allows providing a description of the CO and H₂ adsorption on Ru nanoparticles at an atomistic level.

Results and Discussion

Catalysts characterization.

Silica-supported Ru nanoparticles (RuNPs) were prepared through the same approach on three types of silica-supports, porous, mesoporous and non-porous: incipient wetness impregnation (IWI) of an aqueous solution of [Ru(NO)(NO₃)₃] on aforementioned supports followed by drying in a flow of synthetic air at 120 °C for 12 h and reduction in pure H₂ (99.9999 % and purified over R3-11 BASF catalyst/MS 4Å prior to use) at 400 °C for 6 h (38 mL/min). Table 1 summarizes the main characteristic of each support and silica-supported RuNPs, namely support surface area, Ru-loading, Ru density and particle size.

Table 1. Summary of the N₂-adsorption and HAADF-STEM results on supported RuNPs

Sample	S _{BET} [m ² /g] ^a	Ru loading [%wt.]	Density of Ru [Ru/nm ²]	d RuO ₂ [nm] ^b	d Ru(0) [nm] ^c
Ru/SiO ₂	200	3	0.9	2.1 ± 0.6	1.6 ± 0.6
Ru/SBA-15	800	15	1.1	2.0 ± 0.6	1.5 ± 0.6
Ru/SiO ₂ - spheres	35	0.3	0.5	1.9 ± 0.5	1.4 ± 0.5

^a BET surface area calculated from the N₂ adsorption measurement at -196 °C.

^b Mean particle size obtained from HAADF-STEM analysis of RuNPs assuming full oxidation of RuNPs (RuO₂)¹⁹.

^c Mean particle size of Ru(0) calculated from the difference in molar volume of RuO₂ and Ru(0)

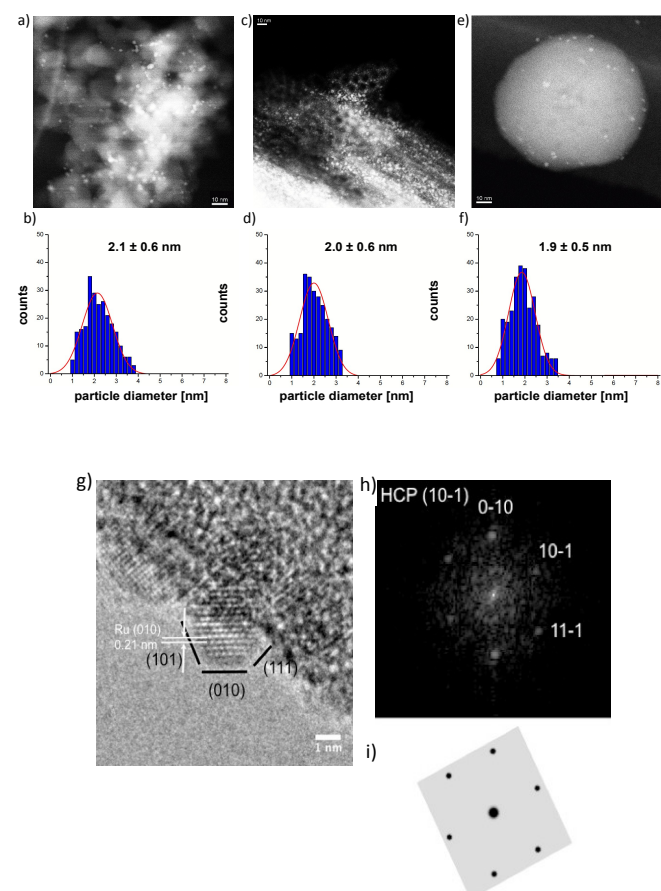


Figure 1 HAADF-STEM of supported RuNPs: a) Ru/SiO₂; b) corresponding particle size distribution for Ru/SiO₂; c) Ru/SBA-15; d) corresponding particle size distribution for Ru/SBA-15; e) Ru/SiO₂-spheres; f) corresponding particle size distribution for Ru/SiO₂-spheres. g) HR TEM of Ru/SiO₂-spheres (0.3 % Ru); h) Fast Fourier Transformation of the corresponding HR TEM image; i) Theoretical diffraction pattern of *hcp* geometry.

The surface area (S_{BET}) of studied supports obtained by N₂ – adsorption exhibit values of 200 m²/g, 800 m²/g and 35 m²/g for SiO₂, SBA-15 and SiO₂-spheres, respectively. In order to obtain comparable density of RuNPs on each support (ca. 1-2 Ru atoms/nm²), three different loadings of Ru were obtained: 3 % wt., 15 % wt. and 0.3 % wt. for Ru/SiO₂, Ru/SBA-15 and Ru/SiO₂-spheres, respectively (Table 1) corresponding to ca. 0.9, 1.1 and 0.5 Ru atoms/nm² for Ru/SiO₂, Ru/SBA-15 and

Ru/SiO₂-spheres respectively assuming that Ru is 100% dispersed and dividing by the total support area.

Hence, all these three materials present rather similar density of Ru atoms and Ru NP's per unit of area. The particle size of RuNPs exposed to air was measured by high Angular Annular Dark Field Scanning Transmission Electron Microscopy (HAADF-STEM) (Figure 1); the mean size diameters are 2.1 ± 0.6 , 2.0 ± 0.6 and 1.9 ± 0.5 for Ru/SiO₂, Ru/SBA-15 and Ru/SiO₂-spheres, respectively. X-ray photoelectron spectroscopy showed that after exposure to air, the oxidation state of RuNPs corresponds to RuO₂ and that under reductive conditions (H₂) the oxidation state of the RuNPs corresponds to Ru(0).¹⁰ Hence, correcting for the difference of molar volume ratio between RuO₂ and Ru(0) (2.35), the mean diameter of Ru(0) nanoparticles can be evaluated to be 1.6 ± 0.6 , 1.5 ± 0.6 and 1.4 ± 0.5 nm for Ru/SiO₂, Ru/SBA-15 and Ru/SiO₂-spheres (Table 1)

The Ru/SiO₂-sphere sample was also investigated by using high-resolution transmission electron microscopy (HR-TEM, Figure 1g) because this support ensures that no metal particles are hidden from view within a pore structure. In addition, it allows the particle morphology to be investigated. Fast Fourier transformation (FFT) analysis of Ru/SiO₂-sphere HR-TEM image allows gaining insight into the diffraction pattern (Figure 1h), which corresponds to the *hcp* structure of Ru (0) (Figure 1i). The sample was not reduced prior HR-TEM study, however the particles adopt *hcp* morphology of Ru(0), presumably because of reduction of Ru under the electron beam. The *hkl* values analysis allows defining the atomic planes of the *hcp* structure: (010), (101), (111). From the distance between the diffraction pattern spots (Figure 1h) the spacing between atomic planes in (010) direction was calculated, which was equal to $d = 0.21$ nm.

H₂ and CO chemisorption measurements

The H₂ isotherms (Figure 2a) exhibit a pressure independent adsorption in the 0 – 15 mbar pressure range, which represents strong chemisorption of H₂ on RuNPs.

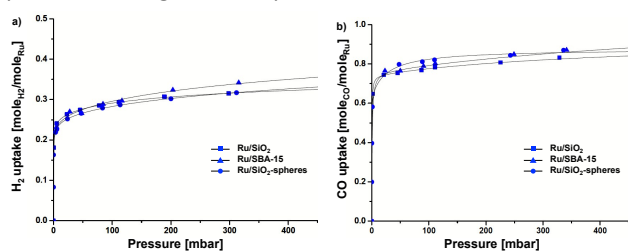


Figure 2 a) H₂ and b) CO - chemisorption isotherms fitted with a dual dissociative Langmuir equation for supported RuNPs.

Above 15 mbar the quantity of adsorbed H₂ increases less significantly with pressure due to physisorption on the support. The H₂ chemisorption data were fitted with dual dissociative Langmuir equation (details in the Supporting Information). CO – chemisorption isotherms are presented in Figure 2b. Similarly to H₂ isotherm, we observe a pressure independent adsorption in the 0 – 15 mbar pressure range, which corresponds to strong chemisorption of CO on RuNPs.

Above 15 mbar the quantity of adsorbed CO increases as a function of pressure corresponding to adsorption on the support. The aforementioned CO chemisorption data was fitted with dual non-dissociative Langmuir model for CO adsorption. Parameters of the Langmuir fit ($Q_{ads,1}$, $Q_{ads,2}$, K_1 , K_2) for both H₂ and CO chemisorption on RuNPs are presented in Supporting Information (SI). Table 2a contains all results from H₂ and CO chemisorption on supported RuNPs. All samples exhibit similar H₂ uptakes. The calculated amount of H₂ adsorbed from the dual dissociative Langmuir equation (Q_{max}) equals 0.62, 0.66 and 0.64 (moleH₂/moleRu) for Ru/SiO₂, Ru/SBA-15, and Ru/SiO₂-spheres respectively. Similarly to the result obtained from H₂ chemisorption, all the samples show comparable CO uptake. The calculated amount of CO (Q_{max}) adsorbed equals 0.94, and 0.96 (moleCO/moleRu) for Ru/SiO₂ and Ru/SBA-15 respectively, and 1.1 (moleCO/moleRu) for Ru/SiO₂-spheres.

Table 2

a) H₂ and CO chemisorption results

Sample	Q_{max} [mole _{H₂} /mole _{Ru}]	Mole Ru ^a	Q_{max} [mole _{CO} /mole _{Ru}]	Mole Ru ^b	Total Mole Ru ^c
Ru/SiO ₂	0.62	2.1×10^{-5}	0.94	2.1×10^{-5}	3.4×10^{-5}
Ru/SBA-15	0.66	6.4×10^{-5}	0.96	6.1×10^{-5}	9.8×10^{-5}
Ru/SiO ₂ -spheres	0.64	4.8×10^{-6}	1.1	5.6×10^{-6}	7.4×10^{-6}

^a Moles of surface Ru based on H₂ chemisorption. ^b Moles of surface Ru based on CO chemisorption. ^c Amount of total Ru moles in corresponding samples used for chemisorption studies.

b) Dispersion (D) and Particle size (d) supported RuNPs.

Sample	D ^a	D ^b	D ^c	d ^a	d ^b	d ^c	d ^d
Ru/SiO ₂	0.62	0.63	0.62	1.6	1.6	1.6 ± 0.6	2.1 ± 0.6
Ru/SBA-15	0.66	0.62	0.66	1.5	1.6	1.5 ± 0.6	2.0 ± 0.6
Ru/SiO ₂ -spheres	0.64	0.75	0.69	1.5	1.3	1.4 ± 0.5	1.9 ± 0.5

^a Based on H₂ chemisorption. ^b Based on CO chemisorption. ^c Based on HAADF-STEM results assuming Ru(0). ^d Based on HAADF-STEM results assuming RuO₂.

The stoichiometry used for the estimation of the particle size was equal to 2H per surface Ru atom for the case of H₂ chemisorption.¹⁹ For the case of CO, the stoichiometry used as 1.5 CO molecules for Ru surface atom according to CO chemisorption combined with particle size distribution obtained by HAADF-STEM measurements. These experimental stoichiometries match what is found by computational calculations. The calculated dispersion (D) from H₂ and CO chemisorption experiments gave comparable results for all studied samples (Table 2b), i.e. approximately 60% of Ru atoms are present at the surface of a nanoparticle. The relation that has been used to estimate the dispersion of an *hcp* particle for a given particle size is described in the ESI. Assuming the *hcp* geometry of a nanoparticle, it translates to ca. 1.6 nm mean particle size (d), which is in a good agreement

with the value obtained by HAADF-STEM and with the one obtained from *ab initio* calculations, which confirms the validity of the assumption of two H adsorbed for Ru surface atom and 1.5 CO adsorbed per Ru surface atom (*vide infra*).

CO adsorption on supported RuNPs studied by FTIR spectroscopy

Figure 3 presents the IR spectrum of CO adsorbed on Ru/SiO₂. The full spectrum and the subtraction spectrum are provided in the SI. A distribution of bands is obtained, which can be decomposed into six bands centered at 2143, 2082, 2046, 2013, 1960 and 1824 cm⁻¹ (Figure 3a). Bands centered at 2082, 2046, 2013, 1960 cm⁻¹ exhibit the highest relative intensity (95 %) and have been previously assigned in the literature as different linear CO species coordinated to Ru atoms.^{34,35} These linearly bound carbonyls are likely atop adsorbed species on Ru atoms.^{26,36,37}

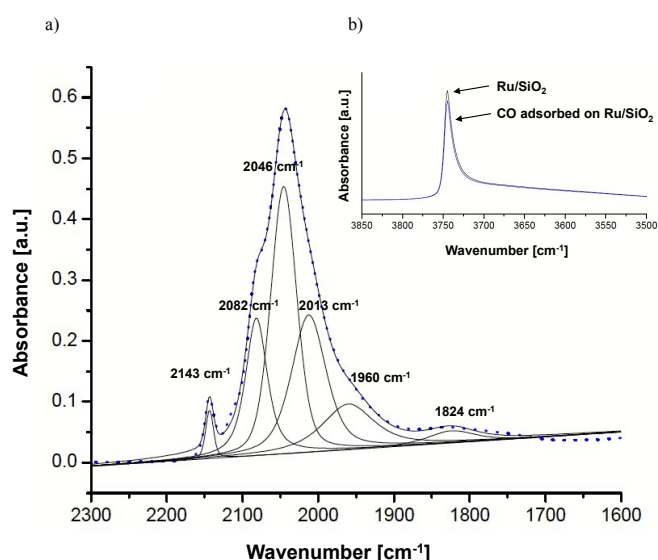


Figure 3. a) CO adsorbed on Ru/SiO₂ studied by IR spectroscopy b) IR of the Silanol groups of the Ru/SiO₂ system with and without adsorbed CO.

The weaker broad band (3 %) observed at lower frequencies (1824 cm⁻¹) is attributed to Ru₂-μ²-CO (bridge-bound) species.^{38,39} The band at higher wave number centered at 2143 cm⁻¹ (2.0%) is not expected for CO species attached to electron rich transition metals, since they classically appear in the range of 2082 to 1960 cm⁻¹ due to back donation of electrons from filled metal orbitals to the antibonding 2π* orbital of CO, which elongates metal-carbon bond and makes it weaker.^{35,40,26} Since the intensity of the ν(OH) is slightly decreased upon adsorption of CO on RuNPs (Figure 3b), thus it is possible that the band at 2143 cm⁻¹ correspond to CO weakly interacting with surface -OH groups of the silica support.

¹³C adsorption on supported RuNPs studied by solid-state ¹³C NMR

Single pulse Magic Angle Spinning (MAS) ¹³C NMR spectrum of ¹³CO coordinated on Ru/SBA-15 was recorded at a spinning frequency of 30 kHz (Figure 4). Ru/SBA-15 was chosen for the

NMR investigation because of the higher loading and thus better signal to noise ratio; the spectrum corresponding to Ru/SiO₂ is provided in the SI. The single pulse spectrum of ¹³CO adsorbed on RuNPs presents 6 isotropic peaks at 172, 181, 190, 195, 197 and 239 ppm. The minor sharp peak at 124.5 ppm corresponds to small amounts of ¹³CO₂.⁴¹

The peak centered at 239 ppm can be assigned to CO adsorbed on the bridging sites of Ru nanoparticles (Ru₂-μ²-CO).^{41,42,43} This resonance is extremely broad (*ca.* 60 ppm) likely due to a wide distribution of chemical shifts, resulting from the variations of local environments at each chemical site of the Ru₂-μ²-CO species. The peaks observed at higher fields (197, 195, 190 ppm) are assigned to linearly bonded CO on RuNPs.^{41,44,45,43} The chemical shift distribution for these species is narrower than the one of the bridge-bonded CO species, probably because it is bound to only one surface Ru atom, thus experiencing less the different environment of particle surface sites. In addition, the resonance at 197 ppm is extremely sharp, suggesting that it corresponds to mobile surface species.

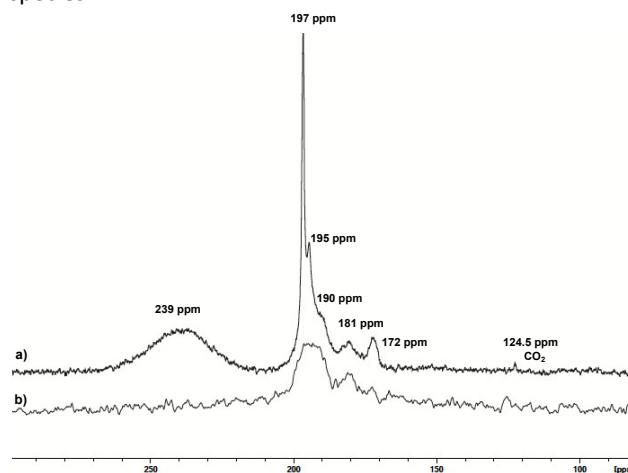
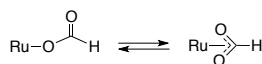


Figure 4 Solid-state ¹³C NMR spectra of ¹³C-labeled CO coordinated on Ru/SBA-15 recorded at 30 kHz spinning rate at a magnetic field of 16.4 T (700 MHz): a) Single ¹³C pulse π/2 excitation with proton decoupling. The radiofrequency field for ¹³C was set to 125 kHz and Spinal-64 proton decoupling was applied during acquisition at a radiofrequency field of 41 kHz. 80k scans were recorded with a recycling delay equal to 0.75 sec. b) CP-MAS spectra recorded with a ¹H radio-frequency field set to 110 kHz, a contact time equal to 3 msec, a recycling delay equal to 2 sec, 30 k scans were used. The radiofrequency field for ¹H decoupling was 110 kHz.

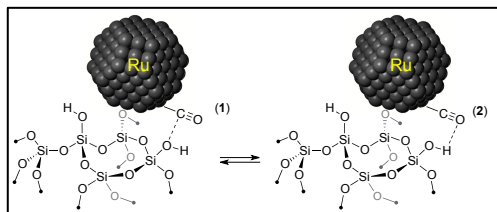
According to the literature, the chemical shift of a peak centered at 197 ppm agree with the chemical shift of multicarbonyl CO species present on Ru nanoparticles.^{44,46} The signal at 172 ppm is consistent with the presence of ruthenium formate species, Ru-(O(O)CH) (see Scheme 1a).^{47,48,49,50} A possible explanation for its presence is the formation of formate through reaction of ¹³CO₂ – observed by solid-state NMR – with ruthenium hydrides.

Scheme 1. a) Proposed Ru-formate species and b) Schematic representation of CO species adsorbed on RuNPs interacting with -OH groups terminating the support surface.

a)



b)



The presence of surface hydride could result from remaining chemisorbed hydrogen even upon pretreatment of the sample at 350 °C and 10^{-5} mbar prior adsorption of ^{13}C O, or alternatively being formed by reaction of surface silanol groups with surface Ru atoms in contact with the silica surface. As for the peak at 181 ppm of weak intensity, we propose that it might originate from a linearly bonded CO species, shifted up-field due to the interaction with the -OH groups terminating the support surface (Scheme 1b).

To evidence whether or not protons (^1H) are located in close proximity to adsorbed CO, carbon-13 Cross-Polarization Magic Angle Spinning (CPMAS) experiments were performed on ^{13}C O coordinated on Ru/SBA-15 (Figure 4b). The CPMAS spectrum displays only some of the peaks observed in the single pulse spectrum, namely the three broad signals at 195, 181 and 172 ppm, that were previously assigned to linearly bonded carbonyl, the carbonyl interacting with OH groups and the putative Ru-formate species. The observation of these signals indicates the presence of protons in their vicinity, that can be either directly bonded protons – like in the case for formate species – or spatially close protons – like surface silanols at the interface between the particle and the support surface. In particular, we note that only a fraction of the linear CO species is observed in the CP-MAS spectrum. The intensity of the peaks at 197 and 195 ppm is especially reduced indicating a high mobility of some of these species (as already pointed out previously) and/or a weak proximity to the surface silanols. We also note that the peak associated with $\text{Ru}_2\text{-}\mu^2\text{-CO}$ (at 239 ppm in the single pulse spectrum) is not observed in the CP MAS spectrum, suggesting that they are located far from any proton, i.e. relatively far from the support, or that they are sufficiently mobile to prevent any efficient CP from protons.

Computational modeling of the CO and Hydrogen-Chemisorption on a Ru nanoparticle

The chemisorption of the CO molecule and the dissociative chemisorption of H_2 were then evaluated on all the possible adsorption sites on a model of an *hcp*-based nanoparticle containing 57 Ru atoms, which corresponds to a particle size equal to 1.1 nm (see Figure 5) and a dispersion equal to 0.77 since there are 44 surface Ru atoms present on the Ru57 nanoparticle. Test calculations for bigger nanoparticles (1.9 nm) suggested that the Ru57 particle is a model that presents a good compromise between accuracy and computational cost.

The stability of different particle shapes has been evaluated, and the results can be found in the supporting information. The selected model of the nanoparticle has two Ru001 planes and twelve Ru101 planes.

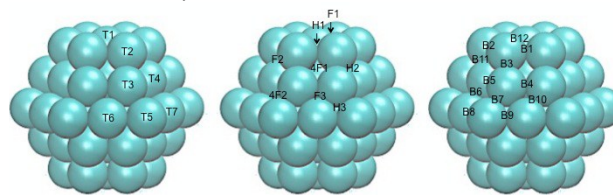


Figure 5. Evaluated adsorption sites on the *hcp* nanoparticle. From left to right: top (T1-T7), three and four-fold sites (H1-H3, F1-F3 and 4F1-2) and bridge sites (B1-B12). There are five kinds of sites where CO and atomic H can adsorb: top sites (T1-T7), bridge sites (B1-B12), *hcp* sites (H1-H3), *fcc* sites (F1-F3) and four-fold sites (4F1, 4F2).

The 111 planes or stepped sites were not included in our model and neither the B5 sites, since they are usually considered not to be present for particle sizes below 2 nm.^{51,52} The Ru101 planes can be divided in two, depending on the number of atoms they contain; either seven or eight Ru atoms. The binding of CO and atomic H on all the possible adsorption sites of the *hcp*-packed nanoparticle was evaluated (Figure 5) Table 3 summarizes the energetics of the binding of CO on the Ru57 nanoparticle. We used the revised version of the PBE functional in order to avoid overestimating the binding energy of CO, which is a common problem of GGA functionals unless significantly more demanding many-body perturbation theory-based methods are used.⁵³ With this functional, we found that the binding energy of CO on the top position of an ideal Ru001 surface is equal to 183 $\text{kJ}\cdot\text{mol}^{-1}$ which it is only slightly higher with respect to the value reported experimentally: 160 $\text{kJ}\cdot\text{mol}^{-1}$. Vibrational contributions to the entropy for CO were not included since they do not contribute significantly to the overall energy at 300 K (e. g. 1.3 $\text{kJ}\cdot\text{mol}^{-1}$ per CO on the T1 site). The most stable adsorption site for the CO molecule corresponds to a top site (T6) of the central atom of one of the horizontal edges between the Ru101 planes located at the third layer of the *hcp* nanoparticle, with a binding energy equal to 212 $\text{kJ}\cdot\text{mol}^{-1}$. The next most stable sites are the T3 and B3 sites, which are located at the vertical edge between two Ru101 planes. These two surface sites have binding energies equal to 202 $\text{kJ}\cdot\text{mol}^{-1}$. Other rather stable positions are the top-positions T1 and T2 and the bridge sites B1 and B2, which have binding energies ranging 190-196 $\text{kJ}\cdot\text{mol}^{-1}$. Finally, one of the *hcp* sites of the Ru101 face (H3) is also quite stable with a binding energy equal to -195 $\text{kJ}\cdot\text{mol}^{-1}$. To summarize, the most stable adsorption sites (with binding energy < -190 $\text{kJ}\cdot\text{mol}^{-1}$) include four 1-fold sites (T1, T2, T3 and T6), three two-fold sites (B1, B2 and B3) and one three-fold site (H3). For the case of atomic H adsorption, which includes zero-point energy corrections, the bridge sites are clearly favored over the rest. Such sites involve the edges of the nanoparticle (B1, B3 and B8) with binding energies within 62-65 $\text{kJ}\cdot\text{mol}^{-1}$.

Table 3. Adsorption energies of the CO molecule and atomic H on all the possible adsorption sites of the *hcp* nanoparticle (in $\text{kJ}\cdot\text{mol}^{-1}$). H adsorption the energies

are referenced to $\frac{1}{2}$ H₂ molecule. Unstable sites evolved to other adsorption sites (these are indicated instead of the binding energy).

Adsorption site	Adsorption Energy CO (kJ.mol ⁻¹)	Adsorption Energy H (kJ.mol ⁻¹)
T1	-193	-28
T2	-196	B1
T3	-202	B3
T4	-149	-28
T5	-171	B8
T6	-212	-35
T7	-177	B8
B1	-190	-62
B2	-191	-55
B3	-202	-65
B4	-164	-40
B5	B3	B3
B6	T5	-23
B7	H3	-55
B8	-185	-63
B9	T6	-45
B10	H3	-55
B11	-157	B2
B12	-166	F1
H1	-168	B1
H2	B3	B3
H3	-195	B7
F1	B2	-57
F2	B2	B2
F3	-175	-49
4F1	B1	-47
4F2	-142	B8

For the case of H₂ the binding energy per H on an ideal Ru001 surface is equal to 59 kJ.mol⁻¹ using the PBE functional. This value is in excellent agreement with the binding energy reported by H₂ desorption experiments on the Ru001 surface (-63 kJ.mol⁻¹).⁵⁴ and also with previously computed values.⁵⁵⁻⁵⁷ Similarly vibrational contributions to the entropy can also be neglected (0.2 kJ.mol⁻¹ per H atom on the F1 site).

CO Chemisorption for different coverages

After having determined the most stable adsorption sites, we optimized structures corresponding to different CO atomic coverages. The coverage is defined as CO molecule per surface Ru atoms of the nanoparticle. We build up the structures based on the following considerations: binding of the adsorbates on the previously determined most stable sites while trying to minimize the repulsion between the adsorbates. We evaluated CO coverages between 0.38 and 1.95 CO ML in order to evaluate the total adsorption energy as a function of the CO coverage. This data is shown in Figure 6a.

We can observe how around 1.9 CO ML the CO adsorption is no longer favored. Hence, based on *ab initio* calculations and without including entropic corrections, we can already suggest that at high P_{CO} , the maximum CO coverage will be around ca. 1.9 CO molecules per Ru surface atom.

A summary for the most stable geometries found for some selected CO coverages (0.5 ML, 1ML, 1.5 ML, 1.61, 1.75 and 1.95 CO ML) are shown in Figure 6b.

For a 0.5 CO ML coverage, two possibilities have been considered (see Figure S1) with either CO binding on the most stable top sites previously determined (T3, T6 and half of the T2 sites) or the CO binding on the T6, B3, T1 and B8 sites. For the first case, the binding energy per adsorbed CO molecule is -177 kJ.mol⁻¹, whereas for the latter the binding energy per CO molecule is higher: -187 kJ.mol⁻¹. The geometry of the latter structure is shown in Figure 6b. This already shows how the CO repulsion is playing a role even at low CO coverages since the former configuration is less stable than the latter, although from the results gathered in Table 3 at very low CO coverage (0.02 ML) would have led to expect the opposite trend. Hence, at low coverages is energetically favored to have CO adsorbed not only exclusively on top sites but also in three fold adsorption sites.

For a coverage of 1 ML, we evaluated three structures (see Figure S2), one considering the adsorption on all the top sites and two additional ones based on the most configuration 0.5 CO ML. In the most stable configuration the CO is located in all the T6, T1, B8, T5 and in a mix of B2, B3, B7, T2 and T3 sites (see Figure 6b) with a binding energy per CO molecule equal to -174 kJ.mol⁻¹. This result contrasts with what has been observed for the CO adsorption on the flat Ru001 surface. Neurock and Iglesia reported for this surface the binding energy becomes endothermic for coverages higher than 0.9 CO ML due to the strong repulsion between CO adlayers.²⁶

The most stable configuration of the nanoparticle with 1.5 CO ML had a binding energy per CO molecule equal to -151 kJ.mol⁻¹. The resulting structure contains CO molecules adsorbed on top (terminal) and bridging sites (see Figure 6b). We can notice that for this CO coverage a noticeable deformation of the nanoparticle can be observed, showing that CO adsorption can induce changes on the nanoparticle structure and that under reactive conditions (e. g. CO pressure) the structure of the nanoparticle can distort. In line with the present findings, a previous study by Sautet and Raybaud has shown that for the case a Pt₁₃ nanoparticle supported on γ -Al₂O₃, H₂ induces strong changes in the nanoparticle shape.²⁸ By including the effect of the variation of the chemical potential of CO $\Delta\mu_{CO}$ we took into account that each adsorbed species is in equilibrium with its respective gas reservoir of CO molecules. Hence, we obtained the stability of a given coverage of CO for a range of $\Delta\mu_{CO}$, which is shown in Table 4.

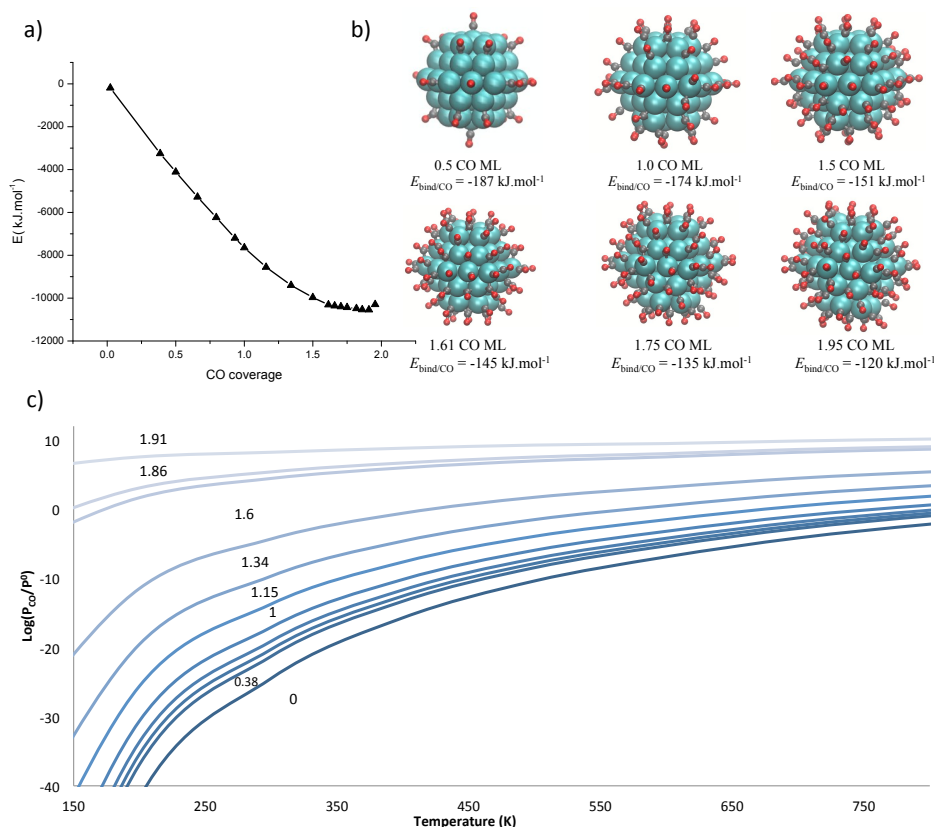


Figure 6 a) Total adsorption energy of on the hcp-based nanoparticle as a function of the CO coverage per Ru surface atom. Energies in $\text{kJ}\cdot\text{mol}^{-1}$. b) Most stable configurations for the coverages equal to 0.5, 1.0, 1.5, 1.61, 1.75 and 1.95 CO ML. The binding energy per CO molecule is also given. c) Areas, in which one given CO coverage is the most stable phase as a function of the $\log(P_{\text{CO}}/P^0)$ and the temperature and the temperature (T , in K).

Table 4. Preferred coverage of CO as function of the variation of the chemical potential: $\Delta\mu_{\text{CO}}$ (in $\text{kJ}\cdot\text{mol}^{-1}$)

Range of stability ($\Delta\mu_{\text{CO}}$, in $\text{kJ}\cdot\text{mol}^{-1}$)	CO coverage (ML)
$\Delta\mu_{\text{CO}} \leq -1.98$	0
$-191 \leq \Delta\mu_{\text{CO}} \leq -173$	0.38
$-173 \leq \Delta\mu_{\text{CO}} \leq -167$	0.5
$-167 \leq \Delta\mu_{\text{CO}} \leq -160$	0.66
$-160 \leq \Delta\mu_{\text{CO}} \leq -149$	0.93
$-149 \leq \Delta\mu_{\text{CO}} \leq -129$	1
$-129 \leq \Delta\mu_{\text{CO}} \leq -106$	1.15
$-106 \leq \Delta\mu_{\text{CO}} \leq -75$	1.34
$-75 \leq \Delta\mu_{\text{CO}} \leq -25$	1.6
$-25 \leq \Delta\mu_{\text{CO}} \leq -19$	1.66
$-19 \leq \Delta\mu_{\text{CO}} \leq -3$	1.86
$\Delta\mu_{\text{CO}} \geq -3$	1.91

We can observe that the coverage that has a broader chemical potential range of stability is the 1.6 CO ML with range for the variation of the chemical potential between -75 and -25 $\text{kJ}\cdot\text{mol}^{-1}$. This means that this coverage will be stable under a broad range of P_{CO} and temperatures since the variation of the chemical potential is related with the pressure of the gas reservoir and the temperature.

This allows to predict the expected CO coverage on the nanoparticle under a given CO pressure and temperature (Figure 6c). Note that this diagram was built based on taking only the most stable coverages for given values of the variation of the chemical potential ($\Delta\mu_{\text{CO}}$) (see ESI). This diagram shows that we have a broad area of P_{CO} and temperature, where the expected CO coverage is equal to 1.61 ML. This area includes the standard conditions ($P_{\text{CO}}=1\text{atm}$ is when $\log P_{\text{CO}}/P^0$ is equal to 0 and $T=298.15\text{K}$). Hence under standard conditions *ab initio* atomistic thermodynamics predicts the most stable phase contains

around 1.6 CO ML. This result agrees well with the coverage determined by chemisorption on the experimentally evaluated systems, which was equal to 1.5 CO ML (vide supra). Note that we have to increase significantly the pressure of CO (around 10^5 atm for temperatures at 300K) in order to get to the next significant area, which corresponds to the 1.86 CO ML coverage. For instance, at $T = 546$ K (275 °C) and $P = 1$ bar, the most stable coverage for CO is equal to 1.34 CO ML, and increasing the temperature around 300 °C, the CO coverage is predicted to decrease to 1.15 CO ML.

This result suggests that when evaluating the reactivity of CO and H₂ on supported Ru nanoparticles in the methanation reaction or Fischer-Tropsch process, coverage between 1.1-1.4 CO ML should be taken into account. In addition, considering the much higher chemisorption energies of CO compared to H, Ru nanoparticles will be mainly covered by CO in a H₂/CO stream or upon exposure to CO of Ru nanoparticles covered with H₂. It is thus not surprising that in reaction involving the conversion of CO, CO is also an inhibitor of the reaction (negative order) and

that upon exposure to CO, H₂ is released from nanoparticles. Concerning lower coverages, for a temperature equal to 300 K, the 0.4 CO ML becomes stable already at very low $P_{CO} = 10^{-25}$ atm. At the same temperature, the 1 CO ML phase becomes stable at rather low CO pressures; e.g. $P_{CO} 10^{-20}$ atm while the 1.5 CO ML is stable from $P_{CO} = 10^{-10}$ atm.

H Chemisorption for different Coverages

For H adsorption on RuNP, the evaluation of the different coverages is more straightforward since the most stable sites are clearly the bridge sites at the edges of the nanoparticle (as shown previously in Table 3). The coverage is defined as H atom per surface Ru atoms of the nanoparticle. The plot of the total adsorption energy as a function of the H coverage including additional intermediate coverages (0.25, 0.75 and 1.25 H ML) shows that saturation of the adsorption sites (no adsorption of additional H₂) corresponds to a coverage close to 2 H ML (Figure 7a).

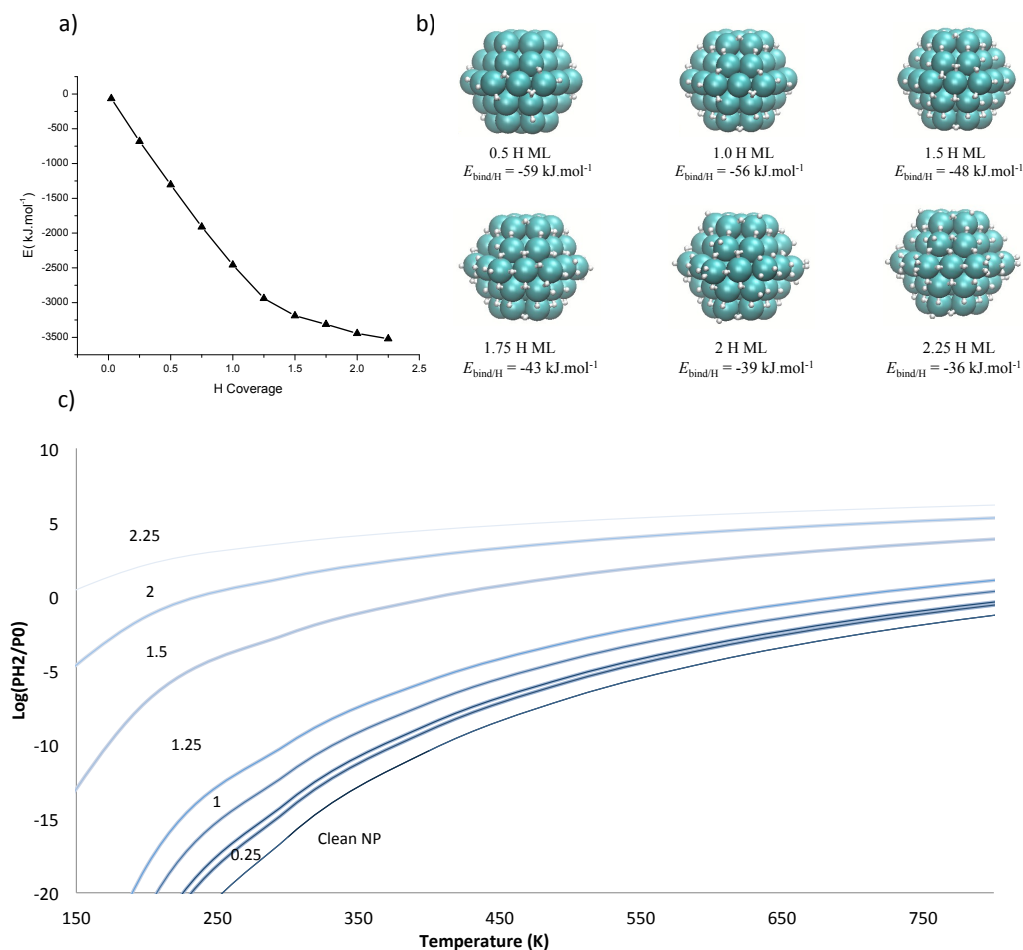


Figure 7. a) Adsorption energy of atomic H on the hcp-based nanoparticle as a function of the H coverage per Ru surface atom. Energies in kJ.mol⁻¹. b) Most stable configurations evaluated for H coverages equal to 0.5, 1, 1.5, 1.75, 2 and 2.25 ML on the hcp-based Ru nanoparticle c) Areas, in which one given H coverage is the most stable phase as a function of the $\log(P_{\text{H}_2}/P^0)$ and the temperature and the temperature (T, in K).

At 0.5 H ML coverage the binding energy per H atom for this coverage is equal to -59 kJ.mol^{-1} . Increasing the coverage up to 1 H and 1.25 H ML does not decrease the binding energies significantly, since the respective binding energies per H atom for these coverages are equal to -56 and -53 kJ.mol^{-1} , respectively. For higher hydrogen coverages: 1.5-2.25 H ML, the repulsion between the adsorbates increases significantly, evidenced by the more pronounced decrease in the binding energy per H atom, ranging -48 and -36 kJ.mol^{-1} for 1.5 and 2.25 H ML, respectively. The binding energy for the 1.5 H ML coverage (-48 kJ.mol^{-1}) is much higher than one reported on the literature for the Ru0001 surface: -21 kJ.mol^{-1} .⁵⁶ A recent study has reported a binding energy per H atom equal to -51 kJ.mol^{-1} on a similar Ru₅₅ hcp for a H coverage equal to 1.2 H ML.²⁷ For 2 H ML the binding energy per H atom is equal to -39 kJ.mol^{-1} , whereas for the same coverage on the Ru0001 surface, a value of 14 kJ.mol^{-1} is reported in the literature.⁵⁷ The data here reported, shows how metallic nanoparticles are able to adsorb significantly more hydrogen than ideal metallic surfaces. All selection of the structures for different binding energy per H as well as the corresponding binding energy per hydrogen atom is shown in Figure 7b. For hydrogen, the expected coverage can be evaluated as a function of the variation of the chemical potential of $\Delta\mu_{\text{H}}$ (see Table 5). The graph used to determine the most stable coverage at a given value of $\Delta\mu_{\text{H}}$ is reported on the ESI. Since the variation of the $\Delta\mu_{\text{H}}$ chemical potential is related with the P_{H_2} and the temperature, we can predict which is the most stable coverage as a function of the pressure of H_2 and the temperature, analogously to the CO case. This diagram is depicted in Figure 7c.

Table 5. Preferred H as function of the variation of the chemical potential: $\Delta\mu_{\text{H}}$ (in kJ.mol^{-1})

Range of stability ($\Delta\mu_{\text{H}}$, in kJ.mol^{-1})	H coverage (ML)
$\Delta\mu_{\text{H}} \leq -62$	0
$-62 \leq \Delta\mu_{\text{H}} \leq -57$	0.25
$-57 \leq \Delta\mu_{\text{H}} \leq -55$	0.5
$-55 \leq \Delta\mu_{\text{H}} \leq -50$	0.75
$-50 \leq \Delta\mu_{\text{H}} \leq -44$	1
$-44 \leq \Delta\mu_{\text{H}} \leq -23$	1.25
$-23 \leq \Delta\mu_{\text{H}} \leq -12$	1.5
$-12 \leq \Delta\mu_{\text{H}} \leq -5$	2
$\Delta\mu_{\text{H}} \geq -5$	2.25

At high temperatures and low H_2 pressures ($\log P_{\text{H}_2}/P^0$), the nanoparticle does not contain adsorbed hydrogen. For a temperature of 300K, the 1 H ML is the preferred phase at a hydrogen pressure around $P_{\text{H}_2} = 10^{-12}$ atm. When increasing more the pressure, the 1.25 H ML becomes stable for a long range of pressures: within 10^{-10} and close to 10^{-2} atm. Finally at standard conditions, the most stable phase corresponds to 1.5 H ML per Ru surface atom, although increasing slightly the pressure (around 10^1 atm), the

experimentally found 2 H ML becomes the most stable phase.

Comparison between Experiment and Theory in the CO/H₂ Chemisorption

The surface phase diagrams obtained both for CO and H_2 on the model Ru₅₇ nanoparticle allows comparing the predicted CO and H_2 coverages under standard conditions ($T = 298 \text{ K}$ and $P = 1 \text{ atm}$) with the ones obtained by chemisorption measurements. Under standard conditions, the CO coverage predicted by *ab initio* calculations is equal to 1.6 CO ML, which compares well with the experimentally measured chemisorption: 1.5 CO ML. For H_2 , the measured coverage is ca. 2 H ML and computations predict a coverage lying in between 1.5 and 2 H ML since the boundary between the two coverages is rather close under standard conditions. In order to evaluate the effect of the binding energies with the particle size we computed the binding energy per H of a 1.5 H ML on a 1.9 nm nanoparticle. The binding energy per H is rather similar for a 1.9 nm nanoparticle than for the 1.1 nm nanoparticle: 44 vs. 53 kJ.mol^{-1} without zero-point energy corrections. Hence, this suggests that within 1 and 2 nm the binding energy per H is not significantly size dependent. Despite the complexity of the system (size and possible configurations), the overall agreement between theory and experiment is good, showing that under standard conditions, the particles have CO and H coverages equal to 1.5-1.6 ML and close to 2 ML, respectively.

⁵⁸Computational IR Analysis and Comparison with Experiment

For some selected CO coverages (0.5, 1, 1.5, 1.61 and 1.91 CO ML) we computed the CO frequencies in order to further understand and to assign the experimental IR signals. The compilation of the C-O stretching modes for the different evaluated CO coverages is shown in Figure 8a while the comparison with the IR spectra is shown in Figure 8b. When there is CO coverage equal to 0.5 ML, we have frequencies between 1730 and 1985 cm^{-1} for the vibrations associated with the C-O stretching mode of the adsorbed CO molecules. The frequencies can be divided in two sets. The first set of frequencies between 1730 and 1862 cm^{-1} corresponds to bridge sites where the CO is adsorbed between two Ru atoms while the second set of frequencies correspond to top sites where CO coordinates just one Ru atom; from 1940 to 1985 cm^{-1} . Within this set of frequencies the highest ones correspond to CO molecules adsorbed on edge of the nanoparticles (T6 sites). For coverage equal to 1 ML the C-O stretching bands are shifted to higher values 1815 and 2063 cm^{-1} with the exception of one C-O stretching frequency at 1552 cm^{-1} . In the CO/Ru001 system IR spectroscopy revealed that the C-O stretching shifts from 1984 to 2061 cm^{-1} when increasing the coverage from 0.003 to 0.67 CO ML.⁵⁸ Again, the lowest frequencies correspond to the bridge-sites while the highest frequencies correspond to the top sites. For CO

coverages equal to 1.5 ML, the calculated frequencies are again slightly shifted, with C-O stretching modes taking values between 1833 and 2084 cm^{-1} in rather good agreement with the range obtained experimentally (see Figure 8b). The broad experimental signals probably indicate a distribution of species, related to defects and different facets not studied here. For a CO coverage equal to 1.6 CO ML, the calculated frequencies range 1755 and 2086 cm^{-1} . Except for the peak at ca. 2143 cm^{-1} , observed experimentally and assigned to CO probably in interaction with surface SiOH, most of the distribution of calculated CO frequencies (Figure 8b). Our calculated frequencies are also similar to previously computed ones for molecular $\text{Ru}_3(\text{CO})_n$ ($n = 12, 11, 10, 9$) species.⁵⁹

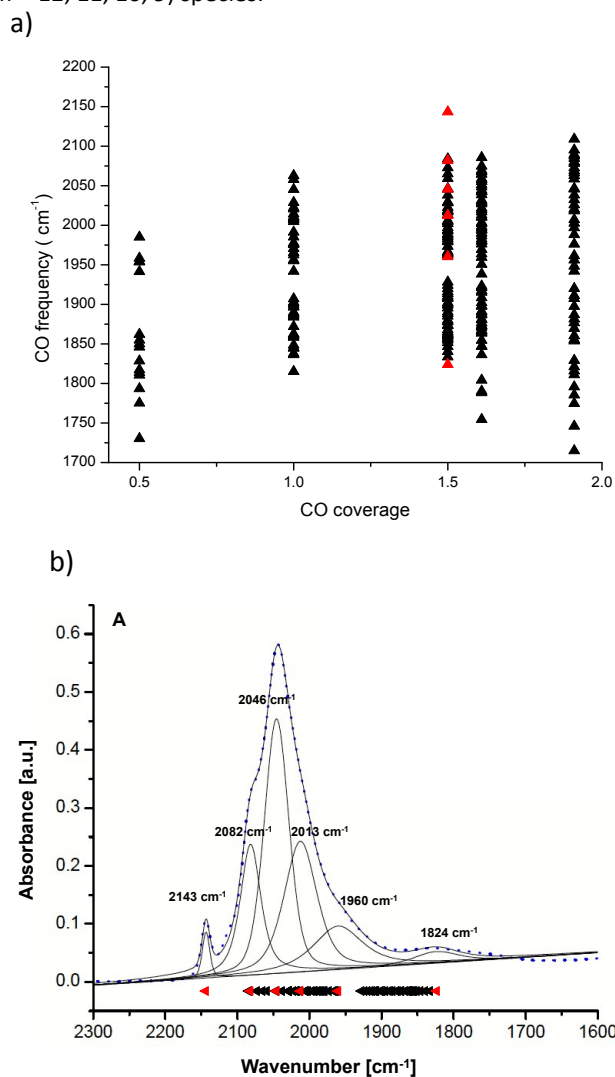


Figure 8. a) Calculated CO stretching frequencies as function of the CO coverage (in black). The experimental CO frequencies for the 1.5 CO ML coverage are highlighted in red. b) Comparison between the experimental signal and the calculated CO stretching frequencies for a CO coverage equal to 1.5 CO ML (as black triangles). The experimental CO frequencies for the 1.5 CO ML coverage are highlighted in red.

Finally, for the coverage at which the nanoparticle is saturated with CO (1.91 CO ML), the frequencies take values between 1715 and 2108 cm^{-1} .

Conclusions

Silica-supported Ru nanoparticles were characterized using H_2 and CO chemisorption, HR-TEM, IR and NMR spectroscopy, and their structural and chemisorption features compared to DFT modeled Ru nanoparticles. HR-TEM images of Ru nanoparticles supported on silica-spheres show the presence of *hcp*-packed nanoparticles, which is also in agreement with the most stable particle shaped predicted by first principles calculations. Hence, the silica support does not alter (influence dramatically) the preferred shape of Ru nanoparticles. Evaluation of the CO and hydrogen coverages of *hcp*-packed Ru nanoparticle as a function of temperature and pressure by *ab initio* atomistic thermodynamics is in good agreement with the experimental results. In particular, the experimental and calculated hydrogen and CO coverages in standard conditions show that the CO coverage on the nanoparticles can reach 1.5-1.6 CO ML, while it is to 2H ML for hydrogen. CO adsorbs on multiple adsorption sites, being coverage dependent, whereas H adsorbs on bridge sites for all the evaluated coverages. While these values greatly exceed what is measured and calculated on flat Ru surfaces, it probably results from the curvature of the nanoparticle, which allows decreasing the repulsion between adsorbates on the surface.

Combining IR spectroscopic data for chemisorbed CO, calculated frequencies and experimental NMR chemical shift of adsorbed CO, one can distinguish different types of chemisorbed CO molecules: bridge-bonded, linear and multicarbonyl CO and possibly ruthenium formate species, all present on the nanoparticle. DFT calculations allow providing an atomistic description of the CO chemisorption in good agreement with experimental IR measurements. As evidenced by solid-state ^{13}C NMR, small portion of linearly bonded CO adsorbed on RuNPs are in a close proximity to the surface silanols, whereas $\text{Ru}_2-\mu^2-\text{CO}$ and multicarbonyl species are likely not in a close contact with the support.

Overall, this detailed study has allowed the evaluation of the preferred morphology of Ru nanoparticles, favoring compact *hcp* structure, and adsorption stoichiometry as a function of temperatures and pressures. This work illustrates in particular the difference of behavior of nanoparticles vs. extended slab surfaces towards CO and H_2 chemisorption. Both experiment and computational calculations shows that the amount of CO and H_2 adsorbed on the Ru nanoparticles are much higher than on flat surfaces, reaching values close to 2 H and 1.5-1.6 CO per surface Ru atom, respectively. Such findings should be taken into account when evaluating the potential energy surfaces and kinetics of the Fischer-Tropsch or methanation reactions by means of *ab initio* calculations. In such reactions, one should consider high coverages of CO (1.2-

1.3 CO ML and low coverages of H in order to properly evaluate the reaction pathways, going beyond the currently used simple slab models. We are currently investigating all these aspects in our lab.

Acknowledgements

We thank the Swiss National Foundation for founding (SNF project number 200021_134775/1 Controlled Surface Chemistry for Catalyst Design and Ambizione project PZ00P2_148059). We are also grateful to Frank Krumeich and Emma Oakton for electron microscopy images, obtained on the ScopeM platform and to Maxence Valla for assistance with the NMR experiments. In addition, we are thankful to GLANTREO Ltd (Ireland) especially Dr. John Hanrahan for providing SiO₂-spheres support. We acknowledge the support from the Swiss National Supercomputing Center for computational resources.

Notes and references

- J. P. Hindermann, G. J. Hutchings and A. Kiennemann, *Catal. Rev.-Sci. Eng.*, 1993, **35**, 1-127.
- H. Schulz and M. Claeys, *Appl. Catal. A*, 1999, **186**, 71-90.
- M. Stelmachowski and L. Nowicki, *Applied Energy*, 2003, **74**, 85-93.
- M. E. Dry, *Catal. Today*, 1990, **6**, 183-206.
- F. Fischer and H. Tropsch, *Berichte der deutschen chemischen Gesellschaft (A and B Series)*, 1926, **59**, 830-831.
- C. Ratnasamy and J. P. Wagner, *Catal. Rev.*, 2009, **51**, 325-440.
- M. A. Vannice, *J. Catal.*, 1977, **50**, 228-236.
- M. A. Gafoor, A. T. Hutton and J. R. Moss, *J. Organomet. Chem.*, 1996, **510**, 233-241.
- M. Che and C. O. Bennett, in *Adv. in Catal.*, eds. H. P. D.D. Eley and B. W. Paul, Academic Press, 1989, vol. Volume 36, pp. 55-172.
- K. Furman, D. Baudouin, T. Margossian, K. D. Sabnis, Y. Cui, F. H. Ribeiro and C. Copéret, *J. Catal.*, 2015, **324**, 9-13.
- B. J. Kip, F. B. M. Duivenvoorden, D. C. Koningsberger and R. Prins, *J. Catal.*, 1987, **105**, 26-38.
- A. D. Allian, K. Takanabe, K. L. Furdala, X. Hao, T. J. Truex, J. Cai, C. Buda, M. Neurock and E. Iglesia, *J. Am. Chem. Soc.*, 2011, **133**, 4498-4517.
- G. Bergeret and P. Gallezot, in *Handbook of Heterogeneous Catalysis*, Wiley-VCH Verlag GmbH & Co. KGaA, 2008, DOI: 10.1002/9783527610044.hetcat0038.
- C. H. Bartholomew and R. B. Pannell, *J. Catal.*, 1980, **65**, 390-401.
- D. G. Mustard and C. H. Bartholomew, *J. Catal.*, 1981, **67**, 186-206.
- J. P. Candy, A. Elmansour, O. A. Ferretti, G. Mabilon, J. P. Bournonville, J. M. Basset and G. Martino, *J. Catal.*, 1988, **112**, 201-209.
- J. Okal, M. Zawadzki, L. Kepinski, L. Krajczyk and W. Tylus, *Appl. Catal. A-Gen.*, 2007, **319**, 202-209.
- R. Prins, *Chem. Rev.*, 2012, **112**, 2714-2738.
- R. Berthoud, P. Délichère, D. Gajan, W. Lukens, K. Pelzer, J.-M. Basset, J.-P. Candy and C. Copéret, *J. Catal.*, 2008, **260**, 387-391.
- M. Lindroos, H. Pfnür, P. Feulner and D. Menzel, *Surf. Sci.*, 1987, **180**, 237-251.
- H. Ahn, C. P. Nicholas and T. J. Marks, *Organometallics*, 2002, **21**, 1788-1806.
- B. Hammer and J. K. Nørskov, in *Adv. in Catal.*, ed. H. K. Bruce C. Gates, Academic Press, 2000, vol. Volume 45, pp. 71-129.
- R. A. Van Santen and M. Neurock, *Catal. Rev.*, 1995, **37**, 557-698.
- R. A. v. Santen, M. Neurock and S. G. Shetty, *Chem. Rev.*, 2009, **110**, 2005-2048.
- R. A. Van Santen and P. Sautet, *Computational Methods in Catalysis and Materials Science*, Wiley-VCH, 2009.
- B. T. Loveless, C. Buda, M. Neurock and E. Iglesia, *J. Am. Chem. Soc.*, 2013, **135**, 6107-6121.
- I. del Rosal, M. Mercy, I. C. Gerber and R. Poteau, *ACS Nano*, 2013, **7**, 9823-9835.
- C. Mager-Maury, G. Bonnard, C. Chizallet, P. Sautet and P. Raybaud, *ChemCatChem*, 2011, **3**, 200-207.
- A. Gorczyca, V. Moizan, C. Chizallet, O. Proux, W. Del Net, E. Lahera, J.-L. Hazemann, P. Raybaud and Y. Joly, *Angew. Chem. Int. Ed.*, 2014, **53**, 12426-12429.
- S. Shetty, A. P. J. Jansen and R. A. van Santen, *J. Am. Chem. Soc.*, 2009, **131**, 12874-12875.
- I. M. Ciobica and R. A. van Santen, *J. Phys. Chem. B*, 2003, **107**, 3808-3812.
- I. A. W. Filot, R. A. van Santen and E. J. M. Hensen, *Angew. Chem. Int. Ed.*, 2014, **53**, 12746-12750.
- D. D. Hibbitts, B. T. Loveless, M. Neurock and E. Iglesia, *Angew. Chem. Int. Ed.*, 2013, **52**, 12273-12278.
- M. F. Brown and R. D. Gonzalez, *J. Phys. Chem.*, 1976, **80**, 1731-1735.
- S. Y. Chin, C. T. Williams and M. D. Amiridis, *J. Phys. Chem. B*, 2006, **110**, 871-882.
- G. Blyholder, *J. Phys. Chem.*, 1964, **68**, 2772-2777.
- T. Mizushima, K. Tohji, Y. Udagawa and A. Ueno, *J. Phys. Chem.*, 1990, **94**, 4980-4985.
- M. E. Bridge, C. M. Comrie and R. M. Lambert, *Surf. Sci.*, 1977, **67**, 393-404.
- M. R. Elahifard, M. Pérez Jigato and J. W. Niemantsverdriet, *Chem. Phys. Lett.*, 2012, **534**, 54-57.
- P. M. Maitlis and V. Zanotti, *Chem. Commun.*, 2009, DOI: 10.1039/b822320n, 1619-1634.
- T. M. Duncan and T. W. Root, *J. Phys. Chem.*, 1988, **92**, 4426-4432.
- F. Novio, K. Philippot and B. Chaudret, *Catal. Lett.*, 2010, **140**, 1-7.
- Y. Gao, M. C. Jennings and R. J. Puddephatt, *Organometallics*, 2001, **20**, 1882-1888.
- T. M. Duncan, K. W. Zilm, D. M. Hamilton and T. W. Root, *J. Phys. Chem.*, 1989, **93**, 2583-2590.
- T. M. Duncan, A. M. Thayer and T. W. Root, *J. Chem. Phys.*, 1990, **92**, 2663-2672.
- A. M. Thayer, T. M. Duncan and D. C. Douglass, *J. Phys. Chem.*, 1990, **94**, 2014-2020.

ARTICLE

Phys. Chem. Chem. Phys.

47. K. Tedsree, A. T. S. Kong and S. C. Tsang, *Angew. Chem. Int. Ed.*, 2009, **48**, 1443-1446.
48. W. Baratta, M. Ballico, A. Del Zotto, E. Herdtweck, S. Magnolia, R. Peloso, K. Siega, M. Toniutti, E. Zangrando and P. Rigo, *Organometallics*, 2009, **28**, 4421-4430.
49. R. Martinez, M.-O. Simon, R. Chevalier, C. Pautigny, J.-P. Genet and S. Darses, *J. Am. Chem. Soc.*, 2009, **131**, 7887-7895.
50. D. H. Gibson, Y. Ding, J. G. Andino, M. S. Mashuta and J. F. Richardson, *Organometallics*, 1998, **17**, 5178-5183.
51. R. van Hardeveld and A. van Montfoort, *Surf. Sci.*, 1966, **4**, 396-430.
52. R. A. Van Santen, *Acc. Chem. Res.*, 2008, **42**, 57-66.
53. L. Schimka, J. Harl, A. Stroppa, A. Grüneis, M. Marsman, F. Mittendorfer and G. Kresse, *Nat Mater*, 2010, **9**, 741-744.
54. P. Feulner and D. Menzel, *Surf. Sci.*, 1985, **154**, 465-488.
55. L. A. Truflandier, I. Del Rosal, B. Chaudret, R. Poteau and I. C. Gerber, *ChemPhysChem*, 2009, **10**, 2939-2942.
56. I. M. Ciobica, A. W. Kleyn and R. A. Van Santen, *J. Phys. Chem. B*, 2002, **107**, 164-172.
57. I. del Rosal, L. Truflandier, R. Poteau and I. C. Gerber, *J. Phys. Chem. C*, 2010, **115**, 2169-2178.
58. H. Pfnür, D. Menzel, F. M. Hoffmann, A. Ortega and A. M. Bradshaw, *Surf. Sci.*, 1980, **93**, 431-452.
59. B. Peng, Q.-S. Li, Y. Xie, R. B. King and H. F. Schaefer III, *Dalton Trans.*, 2008, DOI: 10.1039/B810710F, 6977-6986.